



**HAL**  
open science

## Lithium Niobate Micro-transducers matrix design

Hala El Rammouz, Farouk Benmeddour, Jamal Assaad, Emmanuel Moulin,  
Lucie Dupont, Nikolay Smagin, Youssef Zaatara, Ziad Herro

► **To cite this version:**

Hala El Rammouz, Farouk Benmeddour, Jamal Assaad, Emmanuel Moulin, Lucie Dupont, et al..  
Lithium Niobate Micro-transducers matrix design. 1st International Conference of Engineering Risk  
(INCER 2019), Apr 2019, Beyrouth, Lebanon. pp.01001, 10.1051/mateconf/201928101001 . hal-  
03594232

**HAL Id: hal-03594232**

**<https://uphf.hal.science/hal-03594232>**

Submitted on 11 Jul 2022

**HAL** is a multi-disciplinary open access archive for the deposit and dissemination of scientific research documents, whether they are published or not. The documents may come from teaching and research institutions in France or abroad, or from public or private research centers.

L'archive ouverte pluridisciplinaire **HAL**, est destinée au dépôt et à la diffusion de documents scientifiques de niveau recherche, publiés ou non, émanant des établissements d'enseignement et de recherche français ou étrangers, des laboratoires publics ou privés.



Distributed under a Creative Commons Attribution 4.0 International License

# Lithium Niobate Micro-transducers matrix design

Hala El Rammouz<sup>1,2\*</sup>, Farouk Benmeddour<sup>1</sup>, Jamal Assaad<sup>1</sup>, Emmanuel Moulin<sup>1</sup>, Lucie Dupont<sup>1</sup>, Nikolay Smagin<sup>1</sup>, Youssef Zaatari<sup>2</sup>, and Ziad Herro<sup>2</sup>

<sup>1</sup>UPHF, CNRS, Univ. Lille, YNCREA, Centrale Lille, UMR 8520 –IEMN, DOAE, F-59313 Valenciennes, France

<sup>2</sup>Université Libanaise, Faculté des Sciences II, Laboratoire de Physique Appliquée, Fanar, Liban

**Abstract.** In this work, a two-dimensional (2D) Lithium Niobate ( $\text{LiNbO}_3$ )  $36^\circ\text{Y}$ -cut micro-transducers ( $\mu\text{T}$ s) matrix design is presented. Two main steps define the fabrication process: electrode deposition and photolithography. These steps are preceded by the optical mask conception, which defines the 2D matrix pattern. In contrary to the one element case, this  $\mu\text{T}$ s matrix allows to automatically scan a desired structure in real time. The  $\mu\text{T}$ s matrix is characterized using an impedance analyzer. Furthermore, the experimental tests carried out in order to demonstrate the matrix functionality at low frequencies [200 - 800] kHz are presented.

## 1. Introduction

Lithium Niobate is a well-known lead-free piezoelectric material. This single crystals can be elaborated in different cut types which affect their properties [1]. It has been widely used in ultrasonic transducers for high frequencies applications [2, 3]. Ultrasonic transducers are used to generate and receive guided ultrasonic waves. For decades, ultrasonic transducers have been assembled into different types of arrays one dimensional (1D), two dimensional (2D) or annular for ultrasonic imaging [4] and nondestructive evaluation [5]. Arrays in their 2D matrix form, offer a reduced inspection time with an increased evaluation quality. They are used for the inspection of defects and delamination of plate and cylindrical structures in future work. The propagation of ultrasonic guided waves is quite complicated in such structures [6]. For that, it is important to focus on low frequencies ( $<1\text{MHz}$ ). In addition, reducing transducers size to the micron scale facilitate their integration into structure. In this work, a  $36^\circ\text{Y}$ -cut  $\text{LiNbO}_3$  ( $36^\circ$ rotated on the Y axis) is used having a pertinent material properties [7] for the design of the 2D micro-transducers ( $\mu\text{T}$ s) matrix. This material have a high coupling coefficient and a high Curie temperature.

The aim of this work is to present a new design of a 2D  $\mu\text{T}$ s matrix adapted to circular sections and to demonstrate that  $\text{LiNbO}_3$   $\mu\text{T}$ s can operate at low frequencies, where the number of guided modes is reduced. To this end, section 2 describes the photomask conception and the matrix fabrication process. Section 3 presents the matrix characterization

---

\* Corresponding author: [Hala.ElRammouz@etu.uphf.fr](mailto:Hala.ElRammouz@etu.uphf.fr)

using an impedance analyzer. The characterization made it possible to identify the electrical resonance frequency of all the  $\mu$ Ts of the matrix and showed that the  $\mu$ Ts have the same resonance frequency, which reveals that no manufacturing defect is present. Finally, the experimental ultrasonic tests carried out using different coupling type are explained in section 4. The results showed that the  $\text{LiNbO}_3$   $\mu$ Ts matrix can operate in the low frequencies range.

## 2. Fabrication process

### 2.1. Photomask conception

Since the study of cylindrical structures defines an interest point, it is essential to start by the conception of the photomask which is designed to fit the cylinder section. The  $\mu$ Ts network is made of groups of 3 matrices connected to each other via metallization, each containing 25 circular  $\mu$ Ts as described below. In each group in the network, the middle matrix has a size of 1mm, while the other two (to its left and right) have a size of 1.5 mm and are used for acquiring electrical signals. The center-to-center spacing between two  $\mu$ Ts is 2 mm (Fig 1).

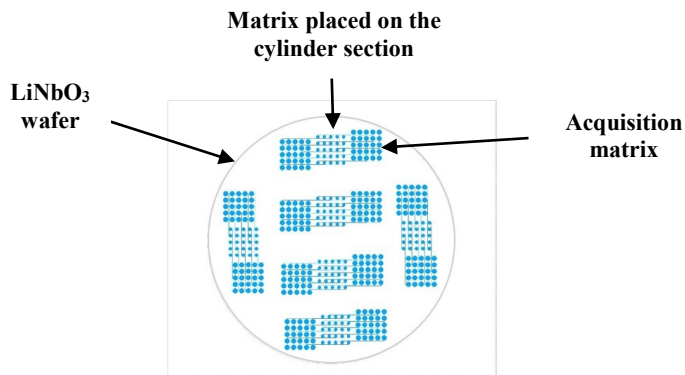


Fig 1. Mask conception

### 2.2. Materials and methods

The  $\mu$ Ts matrices are made using the piezoelectric  $\text{LiNbO}_3$  single crystal  $36^\circ\text{Y}$ -cut wafers with 76 mm diameter and 0.5 mm in thickness. As said, the  $\mu$ Ts are circular in shape and have a width of 1 mm and 1.5 mm (see Fig 1).

The first step is to make the first common electrode of all  $\mu$ Ts which is equivalent to metallizing a face of the wafer with gold [Fig 2 (a)]. An intermediate layer of chromium of 20 nm in thickness is deposited to ensure adherence. Gold is chosen because of its color, which allows to clearly visualize the matrices model. In addition, the gold layer makes it possible to weld gold wires in order to acquire the electrical signals. For this, a minimum thickness of 400 nm of gold is necessary. A thickness of 200 nm was chosen since for now no welding will be performed.

The second step includes several sub steps that are accomplished on the non-metallized wafer face. First, the wafer is dehydrated by putting it on a hot plate at  $110^\circ\text{C}$  for 5 minutes. Then a negative photoresist layer (AZnLOF2020) of 2  $\mu\text{m}$  in thickness is deposited [Fig 2 (b)] using the spin coating technique. The deposition is immediately followed by a thermal annealing of  $110^\circ\text{C}$  during 90 s in order to reinforce the bonds between the molecules of the photoresist. After that, the photolithography process begins [Fig 2 (c)]. The optical mask is placed on its support and a vacuum is applied. After that, the mask is centered and a hard

type exposure is chosen for 7 s. The wafer is placed on the support and the process is launched. Once the UV exposure is done, a thermal annealing at 110°C during 90s is performed. The thermal annealing enhances the resist development and reinforces the bonds where the wafer has been exposed. The resist is developed which means removing the non-exposed photoresist part [Fig 2. (d)]. For that, the wafer is placed in a developer solution (A326) during 90 s and then placed for 30 s in distilled water to ensure cleaning all the resist residue. Once the resist development procedure is done, the second electrode is deposited with the same thickness [Fig 2 (e)]. The last step, called "lift off", consists of cleaning the wafer after metallization [Fig 2 (f)]. This step removes the deposited metal outside the active sites. Cleaning is done with an "SVC remover". The solvent is heated to 65°C. The wafer is immersed in the solvent for a few hours. To avoid reattachment of dissolved gold residue to the substrate, a magnetic bar is placed in the solution. To finish the cleaning procedure, the substrate is immersed in acetone and then in ethanol. The final state of the wafer is shown in Fig 3.

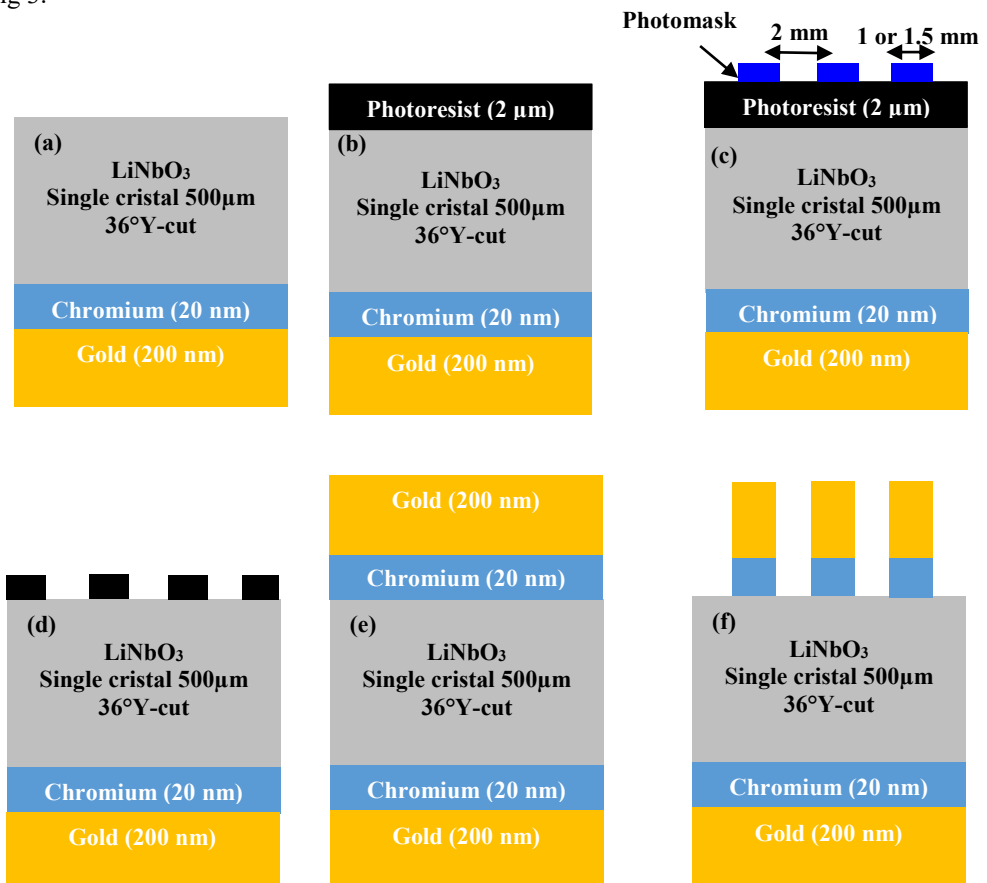


**Fig 2.** Fabrication process: (a) metallization, (b) photoresist deposition, (c) photolithography, (d) photoresist development, (e) metallization and (f) lift off.

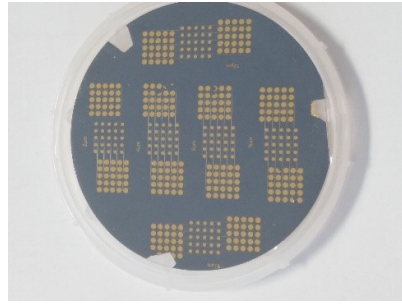


**Fig 3.** Final state of the LiNbO<sub>3</sub> wafer

Sometimes an adhesion problem occurs. Fig 3 shows that on some active sites, the gold has been eliminated by the lift off procedure. This is mainly caused by the resist that did not adhere well to the wafer surface through impurities such as dust. To solve this problem, the substrate is cleaned by placing it in an oxygen plasma.

### 3. Characterization

The aim of this paragraph is to show that all  $\mu$ Ts are identical in order to validate the fabrication process. For this objective, the measurement of the electrical impedance will be shown for different element. The measurements of this electrical impedance will give electrical resonance ( $f_r$ ) and anti-resonance ( $f_a$ ) frequencies, which must be identical for all  $\mu$ Ts. The characterization consists of an impedance analyzer connected to Quarter A-20338 test probes (Fig 4). The matrix is supposed to be free. The applied voltage across the  $\mu$ T is 1V.

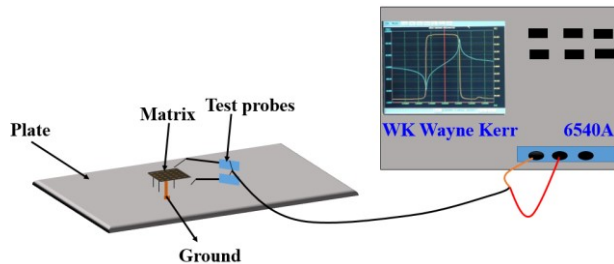


**Fig 4.** Experimental setup to measure the electrical impedance

The impedance is measured on each  $\mu$ T of the matrix and is recorded as a function of frequency. The measurements are divided into 5 series (Fig 5). Here, series 1 and 2 are presented.

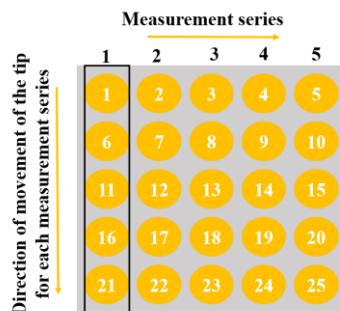


**Fig 5.** Measurements procedure

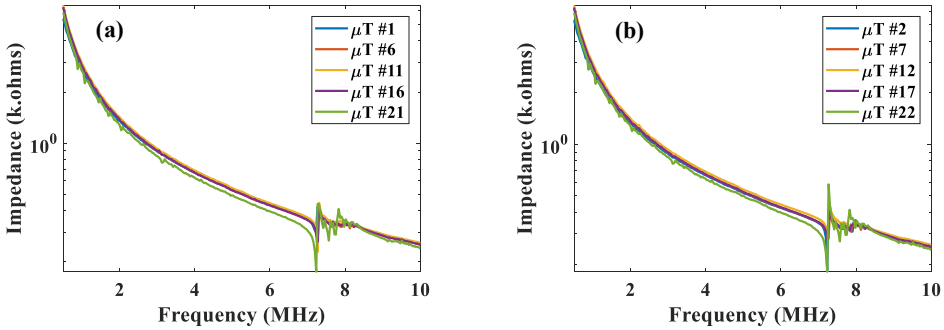


**Fig 6.** Electrical impedance variation versus frequency when the matrix is free: (a) series 1 and (b) series 2

Electric impedance curves have the same allure, which show that all elements are almost the same, and then this validate the fabrication process. The electrical resonance frequency is located between 7.195 MHz and 7.223 MHz. The theoretical value of the mechanical resonance frequency can be computed using one dimensional theory according to the following equation [8]:

$$T = v/2f, \tag{1}$$

where  $T$  represent the piezoelectric material thickness,  $v$  the longitudinal wave velocity in the material and  $f$  the mechanical resonance frequency. The longitudinal velocity in Lithium Niobate is equal to 7340 m/s [9] and the mechanical resonance is equal to 7.340 MHz which is very close to electrical resonance [7]. In addition, Fig. 6 shows weak electrical resonances beyond 0.8 MHz. These results show that no manufacturing defect are present.

In order to show that the matrix can operate at low frequencies, specifically from 100 kHz, the same experimental procedure is performed by fixing the matrix on an aluminum plate ( $50 \times 15 \times 0.6$  cm).

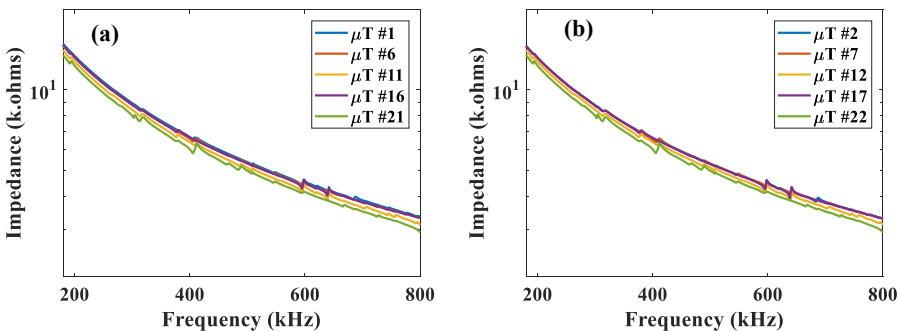


**Fig 7.** Electrical impedance variation versus frequency when the matrix is placed on an aluminum plate: (a) series 1 and (b) series 2

Fig. 7 describes electrical impedance curves and presents weak resonances around 200, 300, 400 and 600 kHz. These resonant frequencies do not define the resonance frequencies of the matrix in air, on the other hand, they are the result of the conjunct resonance of the plate and

the matrix placed on it These results shows that the  $\mu$ Ts matrix is responsive in the low frequency range [180-800] kHz.

#### 4. Experimental tests

As said before, Lithium Niobate transducers have been always used for high frequencies applications. In parallel these transducers has been used for generation and detection of ultrasonic guided waves for structure inspection. Such inspections are quite complicated, that's why working in low frequency domain will reduce its complexity. The aim of this section is to show that the fabricated  $\mu$ Ts matrix can operate at low frequencies. To this end, experimental tests were carried out on an aluminum plate ( $50 \times 15 \times 0.6$  cm). Ultrasonic waves were generated using a Panametrics A413S 0.5/0.5X1.0 transducer with central frequency of 500 kHz. The transmitted frequencies were varied between 20 kHz and 1 MHz with a step of 5 kHz. The excitation signal was a tone burst of 7 cycles and an amplitude of 20 V peak-to-peak. The  $\mu$ Ts matrix was placed at a 19.5 cm from the transmitter. Electrical signals were acquired on each  $\mu$ T in the mentioned frequency range using Quarter A-20338 test probes. This procedure (Fig. 8) was repeated 5 times (Measure 1–5). Each measurement comprises a signal acquisition on all the 25  $\mu$ Ts. First, a petroleum grease was used as a coupling agent. It forms a thin layer between the aluminum plate and the  $\text{LiNbO}_3$  substrate assuring minimal impact of the  $\mu$ Ts matrix on the acoustic waves propagation. Second, the matrix was fixed to the plate with acrylic glue and the same measurements procedure was performed.

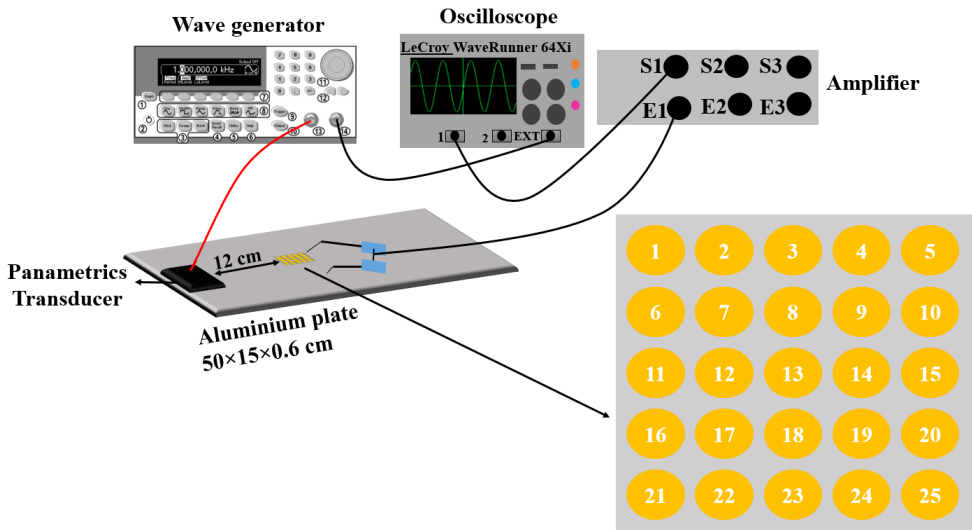
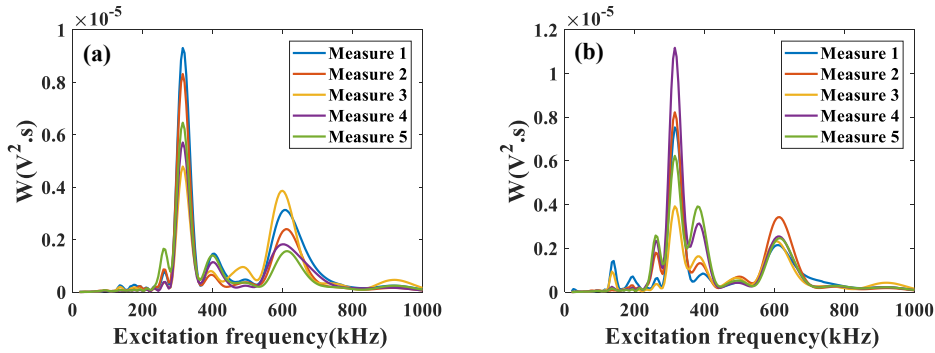


Fig 8. Experimental setup of electrical signal acquisition on each  $\mu$ T.

The signals of the 5 times repeated measurements performed on a single  $\mu$ T are compared by presenting the total energy  $W$  of the signal  $s(t)$  as function of the excitation frequency. The total energy is given accordingly to the following equation [10]:

$$W = \int_{-\infty}^{+\infty} |s(t)|^2 dt, \quad (3)$$



**Fig. 9:** Total energy variation versus excitation frequency using petroleum grease as coupling agent: (a)  $\mu T$  #6 and (b)  $\mu T$  #11.

In the petroleum grease case, the total energy presents two main maxima around 315 kHz and 600 kHz respectively (Fig 9). The total energy value differs between the 5 measurements performed on a single  $\mu T$  and so the results are not repetitive which poses a problem at the acquisition level. This problem is usually attributed to two effects. The first one is that the coupling is not homogeneous between the matrix and the plate. Second, the pressure caused by the test probe on the matrix for each series of measurements performed on the 25  $\mu T$ s is not controllable.

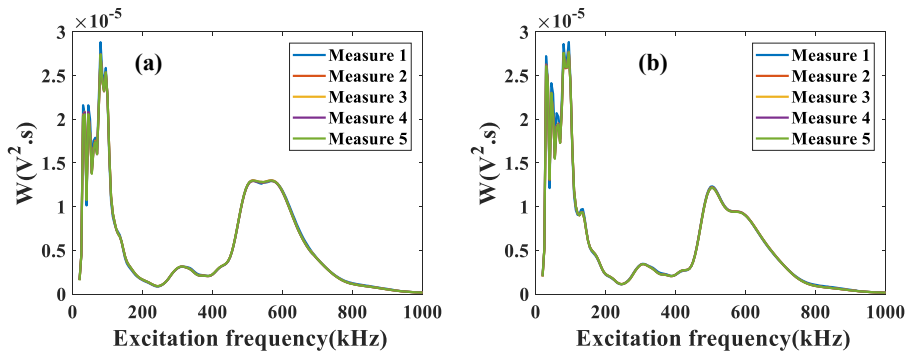


**Fig. 10:** Total energy variation versus excitation frequency using glue as coupling: (a)  $\mu T$  #6 and (b)  $\mu T$  #11

In the second case of a glue-fixed matrix, the total energy curves for 5 different measurements on the  $\mu T$  #6 and  $\mu T$  #11 are almost the same and they have same maxima peaks around 315 kHz and 585 kHz (Fig. 10). The corresponding total energy values for the  $\mu T$  #6 and  $\mu T$  #11 are the same.

Although the results in terms of total energy of the electrical signal differ between the measurements made when using petroleum or acrylic glue, the resonant frequencies are localized around two identical values of 315 and 600 kHz. These resonant frequencies do not correspond to the resonance frequencies of the matrix (section 3), but they are the result of the conjunct resonance of the plate and the matrix placed on it

## 5. Conclusion

In this paper, the fabrication procedure of a 2D Lithium Niobate micro-transducers matrix was presented. The matrix was characterized and the resonance frequency is shown to be

around 7.2 MHz and all the matrix elements are workable. Furthermore, the experimental tests showed that the best coupling to be used is glue because it gives repetitive results. The tests also demonstrate that the  $\text{LiNbO}_3$   $\mu\text{T}$ s matrix can detect signals in low frequency domain especially around 315 and 600 kHz. This must be confirmed soon by other experience. Work under progress is to use this matrix in order to detect defect and delamination in cylindrical structures.

### Acknowledgements

The authors wish to thank the MEAE (Ministère de l'Europe et des Affaires Etrangères), Haut France Region, AUF and the CNRS-L for the funding.

### References

- [1] K.-K. Wong and I. of E. Engineers, Eds., *Properties of lithium niobate*. London: INSPEC/IEE (2002).
- [2] Y. Zhu, N. Ming, W. Jiang, and Y. Shui, *Acoustic superlattice of  $\text{LiNbO}_3$  crystals and its applications to bulk-wave transducers for ultrasonic generation and detection up to 800 MHz*, Appl. Phys. Lett., **53**, no. 15, pp. 1381–1383 (1988).
- [3] Q. Zhou, S. Lau, D. Wu, and K. Kirk Shung, *Piezoelectric films for high frequency ultrasonic transducers in biomedical applications*, Prog. Mater. Sci., **56**, no. 2, pp. 139–174 (2011).
- [4] K. K. Shung and M. Zippuro, *Ultrasonic transducers and arrays*, IEEE Eng. Med. Biol. Mag., **15**, no. 6, pp. 20–30 (1996).
- [5] B. W. Drinkwater and P. D. Wilcox, *Ultrasonic arrays for non-destructive evaluation: A review*, NDT E Int., **39**, no. 7, pp. 525–541 (2006).
- [6] F. Benmeddour, F. Treysède, and L. Laguerre, *Numerical modeling of guided wave interaction with non-axisymmetric cracks in elastic cylinders*, Int. J. Solids Struct., **48**, no. 5, pp. 764–774 (2011).
- [7] J. Assaad, C. Bruneel, J. Decarpigny, and B. Nongaillard, *Electromechanical coupling coefficients and far-field radiation patterns of lithium niobate bars (Y-cut) used in high-frequency acoustical imaging and nondestructive testing*, J. Acoust. Soc. Am., **94**, no. 5, pp. 2969–2978 (1993).
- [8] J. N. Decarpigny, J. C. Debus, B. Tocquet, and D. Boucher, *In-air analysis of piezoelectric Tonpilz transducers in a wide frequency band using a mixed finite element–plane wave method*, J. Acoust. Soc. Am., **78**, no. 5, pp. 1499–1507 (1985).
- [9] J. M. Cannata, T. A. Ritter, Wo-Hsing Chen, R. H. Silverman, and K. K. Shung, *Design of efficient, broadband single-element (20–80 MHz) ultrasonic transducers for medical imaging applications*, IEEE Trans. Ultrason. Ferroelectr. Freq. Control, **50**, no. 11, pp. 1548–1557 (2003).
- [10] P. Stoica and R. L. Moses, *Spectral analysis of signals* (Upper Saddle River, NJ: Pearson, Prentice Hall, 2005).